Pol. J. Environ. Stud. Vol. 34, No. 6 (2025), 8177-8188
DOI: *10.15244/pjoes/195359* ONLINE PUBLICATION DATE: 2025-01-27

Original Research

Hydrogeochemical Analysis of Karst Spring Water Under Highway Construction

Decai Mi[1], Fajia Chen[2, 3], Qiongyao Ye[1], Qiujun Wu[1], Fen Huang[2, 3], Qiang Zhang[2, 3], Bishi Chen[4], Qiong Xiao[2, 3]*

[1]Guangxi Communications Design Group Co. Ltd, Guangxi Nanning 530029, China
[2]Institute of Karst Geology, CAGS/ Key Laboratory of Karst Dynamics, MNR & Guangxi /International Research Center on Karst, UNESCO, Guilin, Guangxi, 541004, China
[3]Pingguo Guangxi, Karst Ecosystem, National Observation and Research Station, Pingguo 531406, China
[4]Yulin No.10 Middle School, Yulin 537000, China

Received: 28 June 2024
Accepted: 28 October 2024

Abstract

Fulong Spring, along K398–K402 in the Hezhou-Bama Highway's Dahua section, was selected for hydrochemical monitoring. This study tracked 13 hydrogeochemical indices, including EC and 6 ions, at 7 sampling points from May 2019 to July 2020. The Piper and Gibbs graphical methods, along with statistical analyses, assessed hydrochemical types, spatiotemporal variations, and controlling factors. The key findings included: ① Fulong Spring has a pH ranging from 6.52 to 10.03 (average 7.22), indicating neutral to alkaline water with Ca^{2+} and Mg^{2+} as dominant cations and HCO_3^- and NO_3^- as principal anions. The hydrochemical type, Ca-HCO_3, reflects the influence of carbonate rock. The water type at the Nongfa Tunnel entrance is Na-K-HCO_3 due to tunnel construction drainage. ② Geochemical indicators in Fulong Basin show minimal seasonal variation, suggesting limited precipitation influence. The tunnel drainage area and Dangui Karst Window show significant spatial differences compared to other points. ③ Most sampling points, except the Nongfa tunnel, exhibit significant water-rock control with minimal precipitation and evaporation influence. However, in the Nongfa Tunnel, carbonate rock dissolution predominantly influences the hydrochemical characteristics. The Nongfa Tunnel is impacted by tunnel drainage and agricultural chemical fertilizer pollution, while the Dangui Karst Window exhibits agricultural fertilization-induced valley sink water contamination.

Keywords: hydrochemical characteristics, tunnel construction, karst, Fulong Spring

Introduction

Karst spring water in the epikarst zone forms part of the near-surface groundwater system. In China's southwestern karst peak cluster region, karst spring water has historically supported populations [1, 2]. The development and utilization of karst spring water are crucial for meeting the needs of residents, livestock, and agricultural irrigation in karst areas with dispersed populations and fragmented lands [3]. Karst spring water can reduce the residence time of infiltrating water in the epikarst system. Good

*e-mail: xiaoqiong-8423@163.com
Tel.: +86-183-7830-0969

vegetation and adequate soil thickness increase infiltration recharge from precipitation. This has played a crucial role in improving and restoring the environment and ecology of karst rocky mountain areas [4]. The southwestern karst region's unique "soil above, water below" structure creates a fragile ecological environment that is hard to restore once damaged [5, 6]. Highway construction in this region has caused a series of ecologically damaging effects, including the pollution of farmland, soil, and water, along with soil erosion. Extensive tunnel and bridge projects have impacted the epikarst zone and deeper karst layers, disrupting the groundwater circulation system to a certain extent [7, 8]. These characteristics give rise to significant challenges in groundwater flow modeling of karstic formations. Further complexity arises when anthropogenic activities such as tunnel construction are involved, where the groundwater flow paths and discharges may change drastically within a short period [9, 10], causing geological and environmental hazards such as mud and water inrush, spring depletion, ground subsidence, and groundwater contamination [11-19].

This study investigates the impact of highway construction on karst spring water. It aims to protect karst water resources and the ecological environment while addressing potential karst hydrogeological hazards during highway construction.

Materials and Methods

Study Area

The Hezhou-Bama Highway is an under-construction highway in Guangxi connecting Hezhou and Bama, passing through Bama, Dahua, Du'an, Mahan, and Xincheng. This region, severely affected by rocky desertification, has an extremely fragile ecological environment, making comprehensive rocky desertification control, ecological restoration, and soil and water conservation particularly challenging. The Dahua section, located in the limestone mountainous area of western Guangxi, is a typically ecologically fragile karst zone with severe poverty and ecological degradation hindering local socioeconomic development. Dahua Yao Autonomous County covers an area of 2,716 km², with karst desertification land covering 1,644.84 km², accounting for 60.2% of the total area. This includes 469.69 km² of severely desertified land, 650.58 km² of moderately desertified land, and 524.57 km² of lightly desertified land. Within the study area, the Hezhou–Bama highway passes through four main tunnels: the Damei, Tongze, Fulong, and Baimen.

Fulong Spring originates in northeastern Guhe Township in Dahua County and is formed by the convergence of four tributaries. It flows 17.6 km into the Hongshui River near Guhe, with a catchment area of approximately 74 km. The groundwater level varies, 20-50 m deep in the upstream section and 0-20 m deep downstream. During the flood season, flow exceeds 10 m³/s, and during the dry season, the flow rate is approximately 0.18 m³/s. These three tributaries intersect the Fulong Tunnel. Dahua County, where the study area is located, is situated in the mid-western part of Guangxi Zhuang Autonomous Region, in the middle reaches of the Hongshui River (107°9′8″–108°8′24″E, 23°56′16″–24°22′15″N). This area lies in the transitional zone between the Yunnan and Guizhou Plateau and the Guangxi Basin, located at the northern edge of the South Asian subtropical climate zone. It receives ample moisture, with annual precipitation ranging from 1249 mm to 1673 mm. The rainy season for the Fulong Spring and its upstream recharge area spans from March to August, with the dry season spanning from September to February.

The study area is predominantly characterized by the development of Carboniferous, Permian, and Triassic strata. The Carboniferous is mainly exposed as follows: the Datang Formation (C_1d) consists of fine-grained sandy dolomitic limestone, thick limestone, and medium-crystalline dolomite, with a thickness of 632 m; the Dapu Formation (C_2d) comprises massive dolomite with occasional intercalations of limestone bands, ranging from 300 to 320 m thick; the Huanglong Formation (C_2h) includes bioclastic limestone, medium-grained sandy limestone, and dolomite interbeds,

Table 1. Overview of Sampling Spring Points.

Sampling sites	Name	Sampling Location	Description
FL1	North Fulong Spring	Outlet of the Fulong underground river	Downstream discharge area
FL2	Middle Fulong Spring	375 m southwest of the under-construction Fulong Tunnel	
FL3	South Fulong Spring	Intake of the centralized drinking water source in Guhe Township	Residential water source
FL4	Groundwater in Karst Window	Dangui Village, outlet 26 m underground	Upstream recharge area
FL5	Nongfa Tunnel Drainage	Drainage point at the Fulong Tunnel entrance	
FL6	Groundwater in Overflow Karst Window	Overflow Karst Window in Nongfa Village, northeast of the Fulong Tunnel entrance	
FL7	Danxian Spring	Hanging Spring in Danxian Village	

with a thickness of 100 to 180 m; and the Upper Carboniferous (C_3) features bioclastic limestone, medium-grained sandy limestone, and dolomite interbeds, with a thickness of 300 to 320 m. The Permian is primarily represented by the Lower Permian Maokou Formation (P_1m), which consists of fine-crystalline limestone interbedded with medium and fine-grained sandy limestone and medium-crystalline dolomite, along with fine-crystalline limestone containing chert nodules, with a total thickness of 640 m. The Triassic is mainly developed in the Middle Triassic (T_2), consisting of calcareous sandstone, shale, and mudstone with minor limestone interlayers. It includes three layers (each over 2 m thick) of tuff and tuff lava, with a total thickness of 305 m [20].

Sampling and Analytical Technique

Fig. 1 shows seven samples collected along the K398–K402 section of the Fulong Spring watershed in Guhe. FL1, FL2, and FL3 are outlets of the Fulong underground river located in the downstream discharge area on the southwest side of the under-constructed Fulong Tunnel. Intake from centralized drinking water sources in Guhe Township. FL3, serving 4,296 people in Guhe Town, is 375 m south of the Fulong Tunnel. FL4, FL6, and FL7 were located in the tunnel entrance area and acted as karst windows in the recharge area of the Fulong Spring. FL4 is a karst window in Dangui Village, with an outlet 26 m underground. FL6 is an overflow karst window in Nongfa Village, northeast of the Fulong Tunnel entrance. FL7 is a hanging spring in Danxian Village. Among these, FL5, which drains from the Fulong Tunnel entrance, was classified separately (Table 1).

Water pH, temperature (T), and dissolved oxygen (DO) were measured in situ using a multiparameter water quality analyzer (YSI 6920, America) with resolutions of 0.01 pH units, 0.01ºC, and 0.001 mg/L, respectively. The HCO_3^- concentration was determined

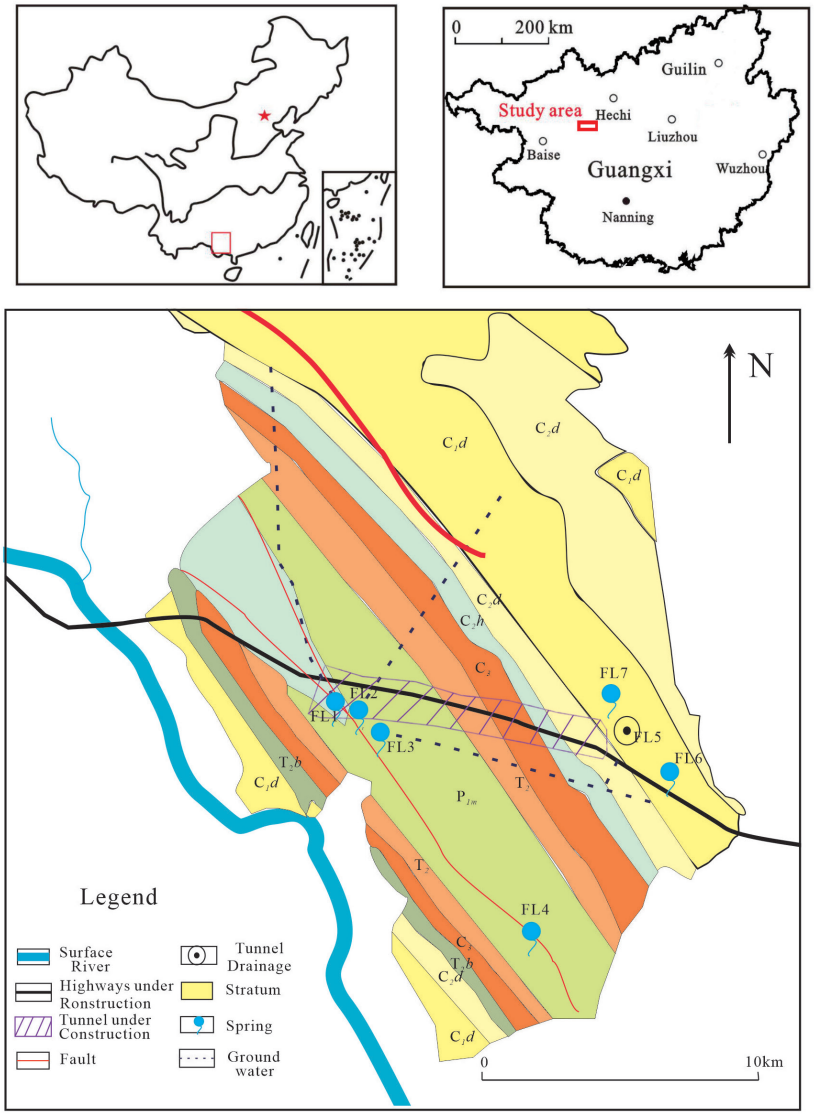

Fig. 1. Location Map of the Study Area.

on-site using a portable test kit (Merck, Germany) with a resolution of 0.1 mmol/L.

Prior to collecting the water samples, the sampling equipment was meticulously selected and purified. To prevent contamination during sampling, the sample bottles were rinsed 3-5 times with water. To avoid air bubbles, the sample bottles were promptly sealed with a film after sampling. Surface water samples collected in the field were filtered through a cellulose acetate membrane with a diameter of 50 mm and pore size of 0.45 μm. Following filtration, cation samples were acidified with HNO_3, sealed, and stored in a dark box. Anion samples were sealed immediately, refrigerated within 12 h of being collected, and stored in a dark box. Analysis of both ions was performed indoors. Anions, such as sulfate (SO_4^{2-}) and chloride (Cl^-), were analyzed using an ICS-900 ion chromatograph, whereas cations, such as potassium (K^+), sodium (Na^+), and calcium (Ca^{2+}), were measured using a Perkin Elmer ICP-OES Optima 2100DV. The analytical errors for the anion and cation analyses were less than 5%. Anion and cation analyses were performed by researchers at the Environmental and Geochemical Laboratory of the Institute of Karst Geology at the Chinese Academy of Geological Sciences.

Results

Karst Spring Hydrochemical Characteristics

Preliminary data analysis indicated Fulong Spring pH values range from 6.52 to 10.03, averaging 7.22, suggesting that the karst spring water was neutral to slightly alkaline. The electrical conductivity (EC) ranges from 168.70 to 498.10 μs/cm, with an average of 416.13 μs/cm. The dissolved oxygen (DO) levels range from 4.24 to 9.52 mg/L, with an average of 7.73 mg/L. Regarding ion mass concentration, the cations are ranked as follows: $Ca^{2+}>Mg^{2+}>Na^+>K^+$, with Ca^{2+} and Mg^{2+} being the predominant cations; the anions are ranked as $HCO_3^->NO_3^->SO_4^{2-}>Cl^-$, with HCO_3^- and NO_3^- being the primary anions.

Piper diagrams of Fulong Spring's major ions during the rainy and dry seasons (Fig. 2a)) revealed distinct ion compositions across the different hydrological periods. During the dry season, the cation composition in the Fulong Spring basin predominantly consisted of Ca^{2+}, accounting for 80-99% of the total cations, with Mg^{2+} comprising 0-20%. Thus, the combined proportion of Ca^{2+} and Mg^{2+} exceeded 90% of the total cations. HCO_3^- dominated, representing 90-99% of the total anion composition, whereas SO_4^{2-} accounted for 0-10%. In the rainy season, the cation composition roughly maintained Ca^{2+} at 70-99% and Mg^{2+} at 0-30%, resulting in a total of over 90% for Ca^{2+} and Mg^{2+}. Anions during this period showed HCO_3^- ranging from 80-99% and SO_4^{2-} ranging from 0–20%, collectively exceeding 90%. More notably, surface runoff exhibits a marked increase during the rainy season as a result of elevated precipitation, accompanied by a slight reduction in the proportions of Ca^{2+} and HCO_3^- and a minor rise in the proportions of other ions. In conclusion, the downstream discharge area, residential water sources, and upstream recharge zone of the Fulong Spring were characterized by Ca-HCO_3 type waters, with carbonate hardness reaching 100%.

The Nongfa Tunnel Drainage (FL5) notably deviated from the other monitoring points in Piper diagrams during both the rainy and dry seasons. An anomalous sample was identified in both periods, characterized by a substantial increase in the concentrations of Na^+ and K^+, altering the chemical type of water to a Na-K-HCO_3 type. This anomaly is likely related to tunnel construction activities, and its specific causes warrant further analysis.

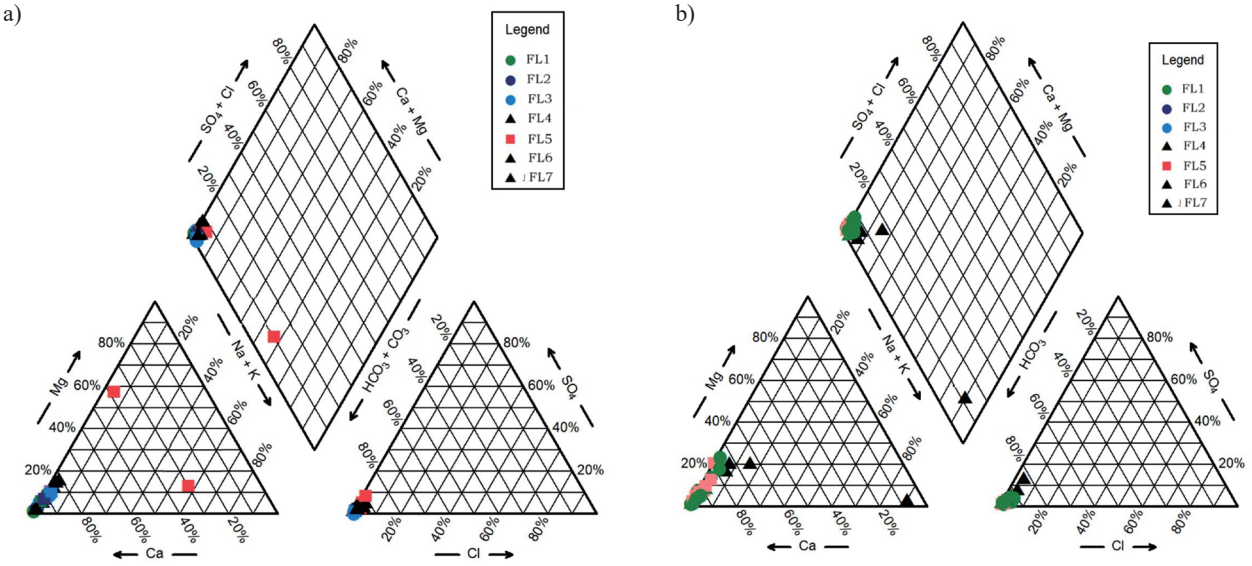

Fig. 2. Piper diagram of Fulong Spring. a) dry seasons; b) rainy seasons.

Spatiotemporal Characteristics of Hydrochemistry in the Fulong Spring

Temporal Variation Characteristics

In the downstream discharge areas of FL1, FL2, and FL3, K^+ and Na^+ trajectories displayed certain similarities. K^+ and Na^+ concentrations in FL1 remained stable from May to August (Fig. 3). In September 2019, they dropped below the detection threshold, but peaked in October at 0.40 mg/L and 1.99 mg/L, respectively. The concentrations subsequently decreased to 0.35 mg/L and 0.6 mg/L, maintaining these levels in the following months. K^+ and Na^+ concentrations in FL2 began to increase in May, peaking in August at 1.06 mg/L and 2.63 mg/L, respectively, before falling to their lowest values in September at 0.18 mg/L and 0.80 mg/L. Thereafter, the levels exhibited a fluctuating upward trend and stabilized. The K^+ and Na^+ concentrations in FL3 showed unusual declines in May, September, and April, with K^+ reaching abnormal levels of 0.51 mg/L, 0.17 mg/L, and 0.35 mg/L, respectively, while other months maintained levels between 0.71 and 0.96 mg/L. The anomalous values for Na^+ were 1.09 mg/L, 0.57 mg/L, and 0.41 mg/L, with other months maintaining levels between 2.16 and 2.82 mg/L. The minor fluctuations in these ion concentrations were not substantial enough to be definitively attributed to wastewater discharge but could be due to the leaching effects of aluminosilicates in the carbonate region. Between May and August, Ca^{2+} rose from 76.03 mg/L to 100 mg/L, with subsequent months fluctuating between 80 and 100 mg/L in FL1. The Ca^{2+} concentrations at FL1 and FL3 remained at approximately 90 mg/L with minor fluctuations. The Mg^{2+} concentration at FL1 was high at 12 mg/L in May, dropping to 0.6 mg/L in September, rising again to 6 mg/L in October, before steadily decreasing to approximately 3.5 mg/L. Concentrations of Mg^{2+} showed anomalies in September and April 2020, dropping to 3.13 mg/L and 1.54 mg/L in FL3, respectively, with other months fluctuating between 4.6 and 6.8 mg/L.

In the recharge area, Na^+ and K^+ concentrations in FL4 showed no significant temporal changes (Fig. 3). The concentration ranges were 0.58-1.66 mg/L for Na^+ and 0.3-0.94 mg/L for K^+. The concentration of Ca^{2+} increased in August, peaked at 112.00 mg/L in September, and then sharply decreased to 44.91 mg/L in October, before rising again and stabilizing. At the Overflow Karst Window, FL6, K^+, and Na^+ concentrations exhibited a fluctuating downward trend from May 2019 to April 2020, reaching lower values of 0.44 mg/L and 0.84 mg/L, respectively, followed by an upward trend. The Ca^{2+} and Mg^{2+} concentrations displayed opposite trends. The K^+ and Na^+ concentrations of FL7 began to increase in September, peaking in April of the following year at 1.25 mg/L and 3.78 mg/L, respectively, and subsequently decreased. The concentration of Ca^{2+} fluctuated downward from May 2019 to July 2020, generally maintaining levels of approximately 95-120 mg/L. The concentration of

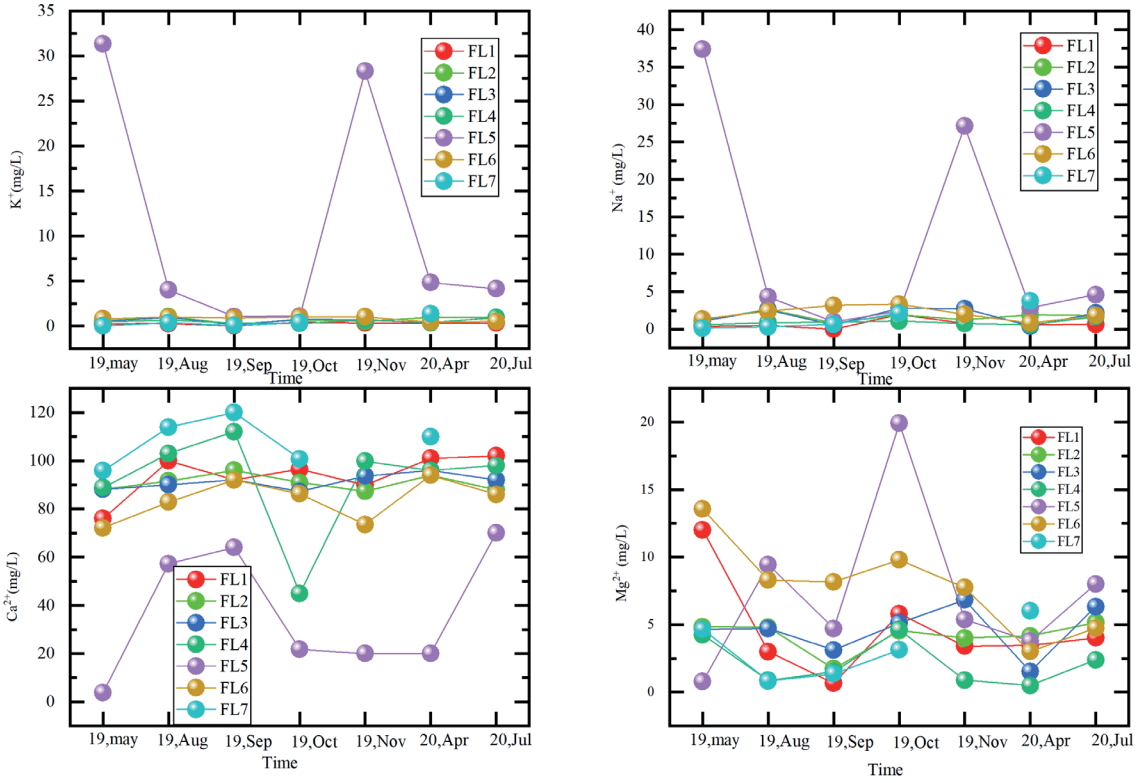

Fig. 3. Time series line graph of cation changes.

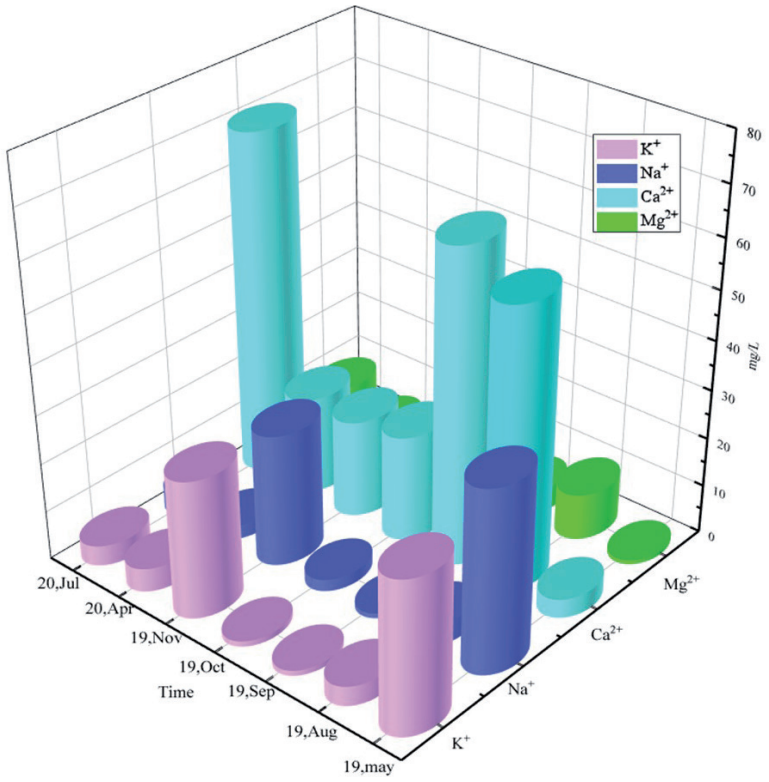

Fig. 4. Time series line graph of cation changes at the Nongfa Tunnel.

Mg^{2+} fluctuated and increased from May 2019 to April 2020, peaking at 6.01 mg/L in April.

The discharge outlet of the Nongfa Tunnel drainage (FL5) was influenced by tunnel construction, leading to elevated concentrations of Na^+ and K^+ in May and November (Fig. 4). Specifically, the concentration of Na^+ reached 37.40 mg/L and 27.13 mg/L, respectively, whereas K^+ peaked at 31.35 mg/L and 28.31 mg/L. The temporal variation curve for Ca^{2+} displayed significant fluctuations; it surged nearly twentyfold to 57.30 mg/L from May to August and remained stable until September. From October 2019 to April 2020, the Ca^{2+} concentration dropped to 20~25 mg/L but recovered to 60 mg/L in July. Fluctuations in Ca^{2+} levels may be associated with the plasma effect caused by the input of other cations (Na^+ and K^+). The Mg^{2+} concentration exhibited minimal changes, with notable fluctuations only in May and October. It reached its lowest at 0.78 mg/L in May and peaked at 19.91 mg/L in October; during other months, it fluctuated between 4 and 9 mg/L.

The SO_4^{2-} and Cl^- concentration curves for the downstream points of Fulong Spring exhibited a high degree of similarity (Fig. 5), suggesting that the influencing factors might have originated from the same source. The concentrations of SO_4^{2-} and Cl^- in FL3 decreased by more than 5 mg/L from August to October, followed by an increase from October 2019 to April 2020. The NO_3^- concentration decreased by approximately 10 mg/L between September and October 2019, whereas the HCO_3^- concentration curve remained relatively stable. The concentrations of SO_4^{2-} and Cl^- in FL1 and FL2 increased from November 2019 to April 2020, with the increase at FL2 and FL3 being relatively more significant than that at FL3. There were minimal seasonal variations in HCO_3^- and NO_3^-. Given that Cl^- is a conservative element and does not participate in chemical weathering, variations in this element, compared to other sampling points, might have been caused by factors other than water-rock interactions.

Variations in the Cl^- and HCO_3^- concentrations were not significant in the two upstream karst windows, FL4, FL6, and Danxian Spring FL7, as illustrated in Fig 6. However, from October to April, the sulfate SO_4^{2-} concentrations increased at FL4 and FL6 and decreased at FL7. From May to September, the NO_3^- concentration at FL4 decreased significantly by over 20 mg/L before increasing, which could be linked to denitrification in an anaerobic environment owing to low dissolved oxygen levels. The concentration returned to its original level by November, and by the rainy season in July, the NO_3^- concentration decreased to near zero owing to dilution effects.

Ion concentrations within the Fulong Springs watershed exhibited substantial variability during the rainy season while remaining relatively stable during the dry season, likely due to the impact of surface runoff on groundwater. Apart from anomalies, K^+, Na^+, and NO_3^- levels in most samples remained stable throughout the year. Concentrations of Ca^{2+}, Mg^{2+}, HCO_3^-, and Cl^- were slightly elevated in the dry season and reduced during the rainy season, reflecting the dilution effect

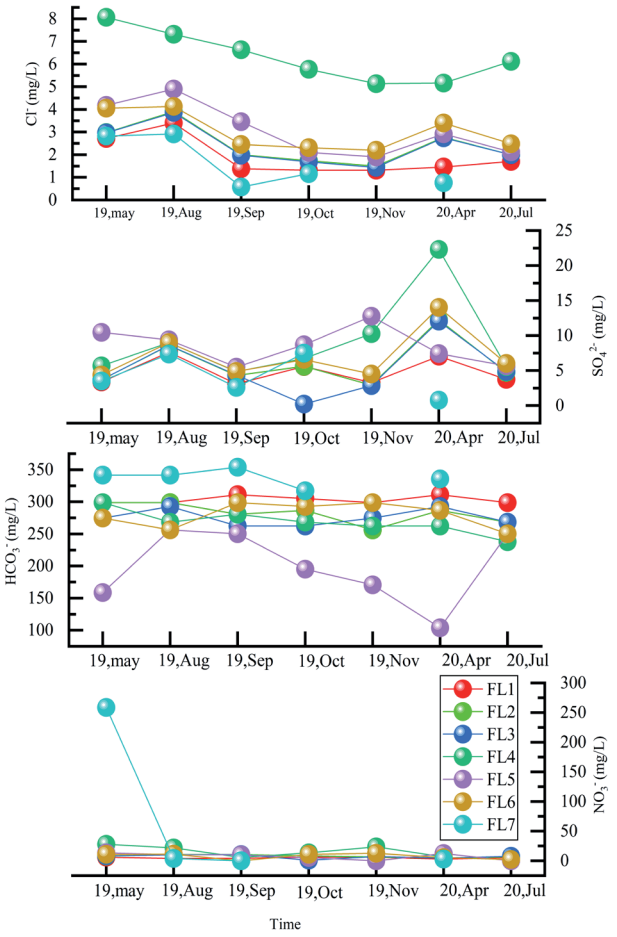

Fig. 5. Time series line graph of anion changes. a) in the Downstream Discharge Area and b) in the Upstream Recharge Area.

of precipitation on groundwater. In contrast, SO_4^{2-} concentrations were marginally higher in the rainy season, possibly due to an increase in sulfate ions from rainfall contributing to groundwater.

Spatial Variation Characteristics

The Na^+ and K^+ concentrations exhibited sudden increases only at FL5, as shown in Fig. 6. An increase in Na^+ concentration above 20 mg/L suggests possible sewage or pollutant intrusion rather than water-rock interactions or precipitation effects. In contrast, the spatial variations in Ca^{2+} and Mg^{2+} concentrations were more complex across the different spring sites, as illustrated in Fig. 6. The differences between the tunnel drainage and karst springs were the most pronounced. Notably, Mg^{2+} experienced an unusual decrease, whereas Ca^{2+} showed significant disparities beginning in October at the Dangui Karst Window compared to other sites, with Ca^{2+} concentrations notably lower than those at other points. In addition, the Mg^{2+} concentration increased in the Overflow Karst Window.

HCO_3^- showed the greatest spatial variation among the four anions, with a significant drop observed in the Tunnel Drainage (FL5), as depicted in Fig. 7. Tunnel construction primarily caused this decline. The other three anions (NO_3^-, Cl^-, and SO_4^{2-}) exhibited no significant differences at FL4 compared with the other spring sites. Notably, the concentrations of NO_3^- and Cl^- increased more markedly at sites other than FL4. This rise could not be explained by water-rock actions alone, with the NO_3^- rise likely stemming from agricultural activities involving fertilizers. In contrast, spatial variations in SO_4^{2-} were not significant and appeared random. This variability was mainly due to the catchment area of FL4, partly originating from the Dangui Village Valley, where agricultural activities and fertilizer application likely raised anion concentrations.

Discussion

The Primary Ion Control Mechanisms in Fulong Spring

The Gibbs diagram facilitated an understanding of the mechanisms contributing to the sources of various cations and anions in karst spring water. It allowed for a qualitative analysis of the trends in ionic changes. As depicted in Fig. 7, the upper-right corner of the diagram represents the control by evaporation and concentration, the middle-left corner indicates water-rock interaction control, and the bottom-right corner reflects precipitation control [21, 22]. The majority of points were positioned towards the middle-left side of the diagram, indicating that water-rock interactions mainly govern the cations and anions in Fulong Spring, typical of karst waters. According to the equations describing karst processes, ions such as Ca^{2+}, Mg^{2+}, and HCO_3^- in water are predominantly influenced by water-rock interactions. Additionally, the Gibbs diagram for the ratio $Na^+/(Na^+{+}Ca^{2+})$ showed that the Nongfa Tunnel (FL5) was subjected to different controlling factors than other sampling points. The ratio of $Na^+/(Na^+{+}Ca^{2+})$ significantly increased, ranging between 0.57 and 0.9 mg/L, with anomalous values noted in May 2019 (0.9 mg/L) and November 2019 (0.57 mg/L). The distribution of points clearly did not follow a trend controlled by evaporation, concentration, or atmospheric precipitation; rather, it was influenced by wastewater discharge from the tunnel construction, leading to an increase in Na^+ concentrations and a decrease in Ca^{2+} concentrations due to plasma effects, causing ionic disarray at this location.

The Analysis of Factors Influencing the Water of Fulong Spring

Correlation Analysis

To validate and analyze the geochemical characteristics of the Fulong Spring and their

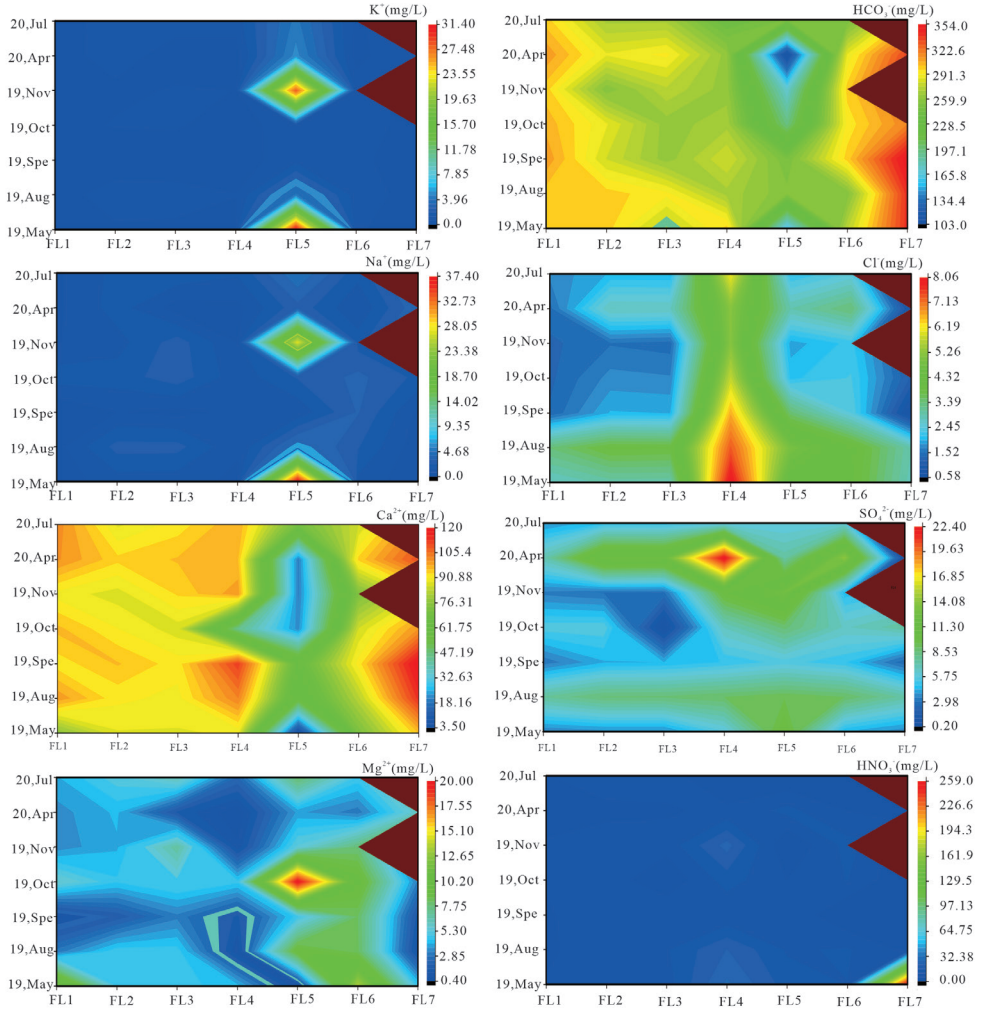

Fig. 6. Line graph of spatial variations in anion concentrations.

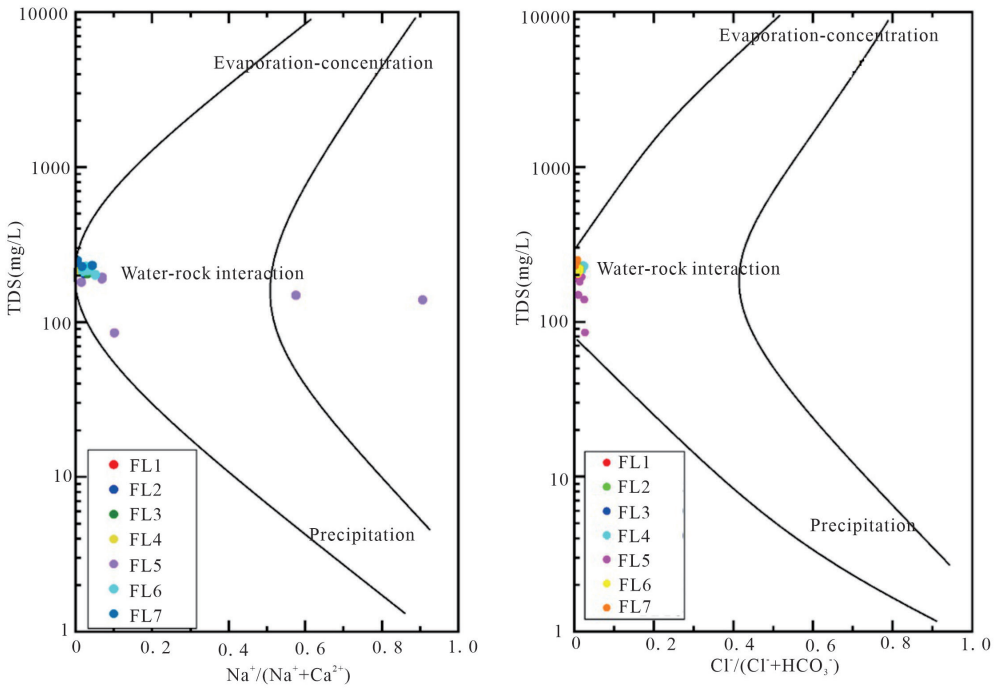

Fig. 7. Gibbs diagram of Fulong Spring.

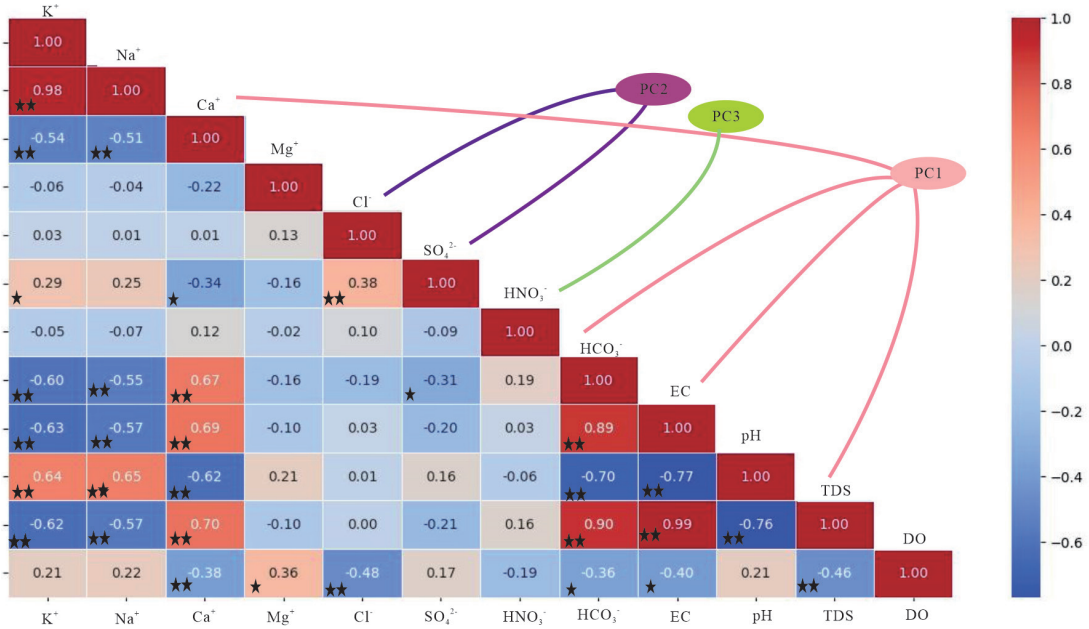

Fig. 8. Significance of correlation analysis of geochemical indicators in Fulong Spring.
Note: ** Correlation is significant at the 0.01 level. * Correlation is significant at the 0.05 level.

interrelations, a statistical correlation analysis was conducted using SPSS 22.0, using 13 parameters collected from May 2019, August to November 2019, and April and July 2020.

As shown in Fig. 8, K^+ exhibited a significant positive correlation with Na^+, SO_4^{2-}, and pH but a slightly less significant correlation with sulfate. K^+ showed a significant negative correlation with Ca^{2+}, HCO_3^-, electrical conductivity (EC), and total dissolved solids (TDS). Na^+ was significantly positively correlated with pH values and significantly negatively correlated with Ca^{2+}, HCO_3^-, EC, and TDS. Ca^{2+} displayed a significant negative correlation with SO_4^{2-} and had significant negative correlations with pH and DO values; it was significantly positively correlated with HCO_3^-, EC, and TDS. HCO_3^- had significant positive correlations with EC and TDS and significant negative correlations with pH, SO_4^{2-}, and DO values. Cl^- showed a positive correlation with sulfate and a negative correlation with DO values.

In analyzing the hydrochemical indicators of the Fulong Spring, K^+ and Na^+ showed remarkably similar direct correlations with other chemical indicators, whereas the correlations between Ca^{2+} and HCO_3^- with other ions significantly overlapped. This indicates that the source mechanisms or influencing factors of these two pairs of ions are consistent, further confirming that the Fulong Spring tunnel is not only influenced by water-rock interactions, but also by external mechanisms.

Fig. 8 shows each geochemical indicator has direct and distinct correlations with the other indicators, complicating the analysis of the influencing factors. Analyzing individual indicators directly results in the loss of information and inaccurate results [23, 24]. Therefore, following the correlation analysis of the hydrochemical indicators of Fulong Spring, dimensionality reduction was performed. Principal component analysis [25, 26] was subsequently employed to further investigate the factors influencing the hydrochemical characteristics.

Principle Component Analysis (PCA)

Using SPSS 22.0, analyses were conducted on Fulong Spring's geochemical indicators. Before principal component analysis, KMO and Bartlett tests were performed, yielding a KMO value >0.6 and a significance level of 0.00, indicating significant correlations and mutual independence suitable for PCA [27, 28]. PCA yielded four components with eigenvalues greater than 1, along with their variance and cumulative contribution rates. The first principal component accounted for 47.148% of the variance, while the remaining three principal components accounted for approximately 10%. The cumulative variance contribution rate was 79.704% (Table 2).

The following presents a detailed analysis of the four principal components. Fig. 8 and Table 3 show

Table 2. Cumulative variance contribution table.

Component	Eigenvalue	Percent variance	Cumulative percentage
1	5.658	47.148	47.148
2	1.650	13.751	60.899
3	1.229	10.239	71.138
4	1.028	8.566	79.704

Table 3. Load table of principal component analysis.

Index	PC1	PC2	PC3	PC4
TDS	0.9212	0.1392	0.0531	-0.1360
EC	0.9143	0.1298	-0.0292	-0.2024
HCO_3^-	0.9102	-0.0532	0.1204	-0.1575
PH	-0.8560	0.0361	0.3162	-0.0236
K^+	-0.8365	0.1211	0.3005	-0.2062
Na^+	-0.8041	0.1145	0.3192	-0.2288
Ca^{2+}	0.8019	0.1294	0.1209	0.0412
Cl^-	-0.0835	0.7779	-0.1825	0.4710
SO_4^{2-}	-0.3664	0.6675	-0.4796	-0.0183
Mg^{2+}	-0.0304	-0.5934	-0.1604	0.5775
NO_3^-	0.1541	0.1181	0.5866	0.5389
DO	-0.5068	-0.3853	-0.5202	-0.0219

the first principal components, TDS, EC, HCO_3^-, and Ca^{2+}, all have loadings greater than 0.8. These four indicators are closely related to carbonate dissolution, indicating that the first principal component primarily reflects the impact of water-rock interactions on Fulong Spring. In the second principal component, the loadings of Cl^- and SO_4^{2-} are 0.7779 and 0.6675, respectively. These indicators are closely related to human activities, including tunnel construction and agricultural activities. In PC3 and PC4, only NO_3^- has a significant load (0.5866). Based on previous analysis, this is attributed to pollution from agricultural fertilization activities in the valley affecting the Dangui Karst Window, as well as the nitrification and denitrification processes resulting from active microbial states in the water under anaerobic conditions.

Factor Analysis of the Nognfa Tunnel

Due to significant spatial differences between the sampling sites in the Nongfa Tunnel and the other sampling sites in Fulong Spring, a separate factor analysis was conducted for the Nongfa Tunnel.

Table 4. Cumulative variance contribution table of Nongfa Tunnel.

Total variance interpretation		
Component	Percent variance	Cumulative percentage
1	54.07	54.07
2	18.71	72.78
3	16.167	88.947
4	8.952	97.899

Based on the PCA, four main factors with eigenvalues greater than one were identified, with a cumulative variance contribution rate of 97.899% (Table 4). This indicated that these four factors reflected 97.899% of the information in the overall sample. The component matrix was rotated using the varimax rotation method, resulting in a rotated factor-loading table (Table 5).

Based on the factor analysis, as shown in the table, the loads of EC, TDS, Ca^{2+}, and HCO_3^- in RF1 are 0.959, 0.961, 0.577, and 0.921, respectively. The primary minerals in the carbonate region are calcite and dolomite. The concentrations of Ca^{2+} and HCO_3^- in water are closely related to karst processes. Therefore, RF1 can be considered controlled by water-rock interactions in the carbonate region. In RF2, the loads of Na^+ and K^+ are 0.828 and 0.793, respectively, whereas that of SO_4^{2-} was 0.973. Previous analyses showed that the concentrations of these three ions do not exhibit significant seasonal variations in response to precipitation, evaporation, or karst processes. The negative loading of Ca^{2+} further excluded the influence of karst processes. Thus, RF2 can be interpreted as reflecting the impact of the Na^+ and K^+ components from tunnel discharge on Nongfa Tunnel sampling. In RF3, only Ca^{2+} and Mg^{2+} have significant loads; therefore, RF3 can be considered to represent the influence of the tunnel discharge containing Ca^{2+} and Mg^{2+} on the Nongfa Tunnel. In RF4, only NO_3^- and Cl^- have significant loads. Based on previous analyses, this factor can be attributed to pollution from agricultural fertilization in the surrounding valley bottom, which affects runoff.

Conclusions

This study investigated Nongfa Tunnel's hydrogeochemical characteristics through monthly

Table 5. Rotation factor (RF) load table.

Index	RF1	RF2	RF3	RF4
EC	0.959	-0.04	0.278	-0.02
PH	-0.24	0.284	-0.83	0.188
TDS	0.961	-0.04	0.272	-0.02
DO	-0.78	0.569	0.18	-0.04
K^+	-0.11	0.828	-0.53	-0.13
Na^+	-0.03	0.793	-0.61	-0.04
Ca^{2+}	0.577	-0.62	0.526	-0.05
Mg^{2+}	0.428	-0.1	0.859	-0.13
Cl^-	0.219	0.07	0.021	0.972
SO_4^{2-}	-0.18	0.973	0.003	0.002
NO_3^-	-0.3	-0.19	-0.29	0.881
HCO_3^-	0.921	-0.22	0.319	0.022

Note: Extraction method: PCA. The rotation converged after 9 iterations.

dynamic monitoring from May 2019 to July 2020. The following conclusions were drawn.

1. The pH of the Fulong Spring ranges from 6.52 to 10.03, with an average of 7.22, indicating neutral to slightly alkaline karst spring water. In terms of the ion mass concentration, the cation sequence was Ca^{2+}> Mg^{2+}>Na^+>K^+, with Ca^{2+} and Mg^{2+} being the dominant ions. The anion sequence is HCO_3^->NO_3^->SO_4^{2-}>Cl^-, with HCO_3^- and NO_3^- dominant. Overall, the water chemistry of the Fulong Spring is of the Ca-HCO_3 type, reflecting the control of carbonate rock formations on the hydrochemistry. Anomalies in the Nongfa Tunnel data indicate a Na-K-HCO_3 type, reflecting the impact of tunnel drainage on Fulong Spring's hydrochemical characteristics.

2. Fulong Spring's geochemical indicator showed no significant seasonal variation, indicating minimal precipitation control. Significant spatial differences were observed among the sampling points, except in the tunnel drainage area and Dangui Karst Window, which differed markedly from the others.

3. According to the Gibbs diagram, all sampling points, except for the Nongfa Tunnel, showed clear water-rock interaction control with minimal influence from precipitation and evaporation concentration. The Nongfa Tunnel results suggest control by factors other than the three aforementioned. Principal component and factor analyses further verified that the primary control factor for the Fulong Spring and Nongfa Tunnels is carbonate rock dissolution. Additionally, the hydrochemical characteristics are influenced by tunnel drainage pollution and agricultural fertilizer pollution, whereas the Dangui Karst Window shows valley runoff pollution is due to agricultural activities.

In summary, Fulong Spring's hydrochemical characteristics were predominantly controlled by water-rock interactions. However, some sampling points exhibited changes in hydrochemical characteristics due to tunnel construction and agricultural activities, leading to complex variations in the hydrochemistry of the Fulong Spring.

Acknowledgments

This work was supported by the Science and Technology Plan Project of Guangxi Province (2022GXNSFAA035572; Guike AB22035010; 2022GXNSFAA035604); the China Geological Survey Project (DD20230547); the China Foreign Experts Bureau Project (DL2023055001L), and the Opening Project of Key Laboratory of Karst Dynamics, Ministry of Land and Resources, Guangxi（No. KDL&Guangxi202208).

Conflict of Interest

The authors declare no conflict of interest.

References

1. YUAN D.X. Scientific innovation in karst resources and environ ment research field of China. Carsologica Sinca. **34** (2), 98, **2015**.
2. LI Z., XU X., YU B., XU C., LIU M., WANG K. Quantifying the impacts of climate and human activities on water and sediment discharge in a karst region of southwest China. Journal of Hydrology. **542**, 836, **2016**.
3. LIANG X.P., ZHU Z.W., LIANG B., GUAN B.Z., ZOU S.Z. Preliminary analysis on hydrogeochemical characteristics of the epikarst zone in luota, hunan. Carsologica Sinica. **2003** (2), 22, **2003**.

4. JIANG Z.C., YUAN D.X. Dynamics Features of the Epikarst Zone and Their Significance in Environments and Resources. Acta Geoscientia Sinica. **1999** (3), 302, **1999**.
5. ZHAO L.S., HOU R. Human causes of soil loss in rural karst environments: a case study of Guizhou, China. Science Reports. **9**, 1, **2019**.
6. XIAO Q., WANG P., WU K.Y. Hydrogeochemical feature of thermal groundwater in carbonate reservoir in Triassic in Chongqing. Resources and Environment in the Yangtze Basin. **24** (8), 1351, **2015**.
7. GAO X.B., WANG W.Z., HOU B.J., GAO L.B., ZHANG J.Y., ZHANG S.T., LI C.C., JIANG C.F. Analysis of karst groundwater pollution in northern China. Carsologica Sinica. **2020** (3), 287, **2020**.
8. XIE G.W., YANG P.H., SHENG T., DENG S.J., HONG A.H. Comparison of the geochemical characteristics of karst springs of a vertically zoned climate region under human activity: a case of Shuifang Spring and Bitan Spring in the Jinfo Mountain area, Chongqing. Environmental Scie.nce, **40** (7), 3078, **2019**.
9. HAO Y., ZHANG J., WANG J., LI R., HAO P., ZHAN H. How does the anthropogenic activity affect the spring discharge? Journal of Hydrology. **540**, 1053, **2016**.
10. LV Y., JIANG Y., HU W., CAO M., MAO Y. A review of the effects of tunnel excavation on the hydrology, ecology, and environment in karst areas: Current status, challenges, and perspectives. Journal of Hydrology. **586**, 124891,**2020**.
11. ZHOU B.Q., YANG Z.B., HU R., ZHAO X.J., CHEN Y.F. Assessing the impact of tunnelling on karst groundwater balance by using lumped parameter models. Journal of Hydrology. **599**, 126375, **2021**.
12. PU J.B., YUAN D.X., HE Q.F., WANG Z.J., HU Z.Y., GOUP.F. High-resolution monitoring of nitrate variations in a typical subterranean karst stream, Chongqing. China. Environment. Earth Science. **64** (7), 1985, **2011**.
13. MAHLER B.J., BOURGEAI R. Dissolved oxygen fluctuations in karst spring flow and implications for endemic species: Barton Springs, Edwards aquifer, Texas. USA. Journal of Hydrology. **505**, 291, **2013**.
14. GRIMMEISEN F., ZEMANN M., GOEPPERT N., GOLDSCHEIDER N. Weekly variations of discharge and groundwater quality caused by intermittent water supply in an urbanized karst catchment. Journal of Hydrology. **537**, 157, **2016**.
15. HAN D.M., CURRELL M.J., CAO G.L., HALL B. Alterations to groundwater recharge due to anthropogenic landscape change. Journal of Hydrology. **554**, 545, **2017**.
16. JIANG Y.J., CAO M., YUAN D.X., ZHANG Y.Z., HE Q.F. Hydrogeological characterization and environmental effects of the deteriorating urban karst groundwater in a karst trough valley: Nanshan. SW China. Journal of Hydrology. **26** (5), 1487, **2020**.
17. LIU J.C., SHEN L.C., WANG Z.X., DUAN S.H., WU W., PENG X.Y., WU C., JIANG Y.J. Response of plants water uptake patterns to tunnels excavation based on stable isotopes in a karst trough valley. Journal of Hydrology. **571**, 485, **2019**.
18. CHEN Y., LIAO Z., ZHOU J., HU R., YANG Z., ZHAO X., WU X., YANG X. Non Darcia flow effect on discharge into a tunnel in karst aquifers. International Journal of Rock Mechanics And Mining Sciences. **130**, 104319, **2020**.
19. ZHOU J., LIU H., LI C., HE X., TANG H., ZHAO X. A semi-empirical model for water inflow into a tunnel in fractured-rock aquifers considering non-Darcian flow. Journal of Hydrology. **597**, 126149, **2021**.
20. YANG Q.Q., WANG K.L., CHEN H.S., ZHANG W., TIAN R.C. Effect of geology and Landform on karst rock desertification: A case study in Dahua County of Guangxi, China. Journal of Mountain Science. **27** (3), 311, **2009**.
21. ZHOU X.Y., HE S.Y., YANG Y.Z., WU P., LUO W. Hydrochemical fingerprints of karst underground river systems impacted by urbanization in Guiyang, Southwest China. Journal of Contaminant Hydrology. **264**, 104356, **2024**.
22. ZHU X.Q., LAN F.N., ZHAO Y., LI Y.Q., LIU P., HOU S.T., WEI M.J., YUE X.F. Hydrochemical characteristics and causes of Nandong karst water system in Yunnan Province. Yangtze River. **52** (5), 37, **2021**.
23. WUNDERLIN D., DIAZ M., AME M., PESCE S.F., HUED A.C., BISTONI M.A. Pattern recognition techniques for the evaluation of spatial and temporal variations in water quality. A case study: Suquia river basin (Cordoba, Argentina). Water Research. **35**, 2881, **2001**.
24. SIMEONOV V., STRATIS J., SAMARA C., ZACHARIADIS G., VOUTSA D., ANTHEMIDIS A., SOFONIOU M., KOUIMTZIS T. Assessment of the surface water quality in northern Greece. Water Research. **37**, 4119, **2003**.
25. MUSTAFA E., MOHAMED W., HEBA F., FAHAD A., FATHY A., RAAFAT M.E. Assessment of groundwater quality in arid regions utilizing principal component analysis, GIS, and machine learning techniques. Marine Pollution Bulletin. **205**, 116645, **2024**.
26. KAMRAN Z., ELNAZ R. Determining spatial and temporal changes of surface water quality using principal component analysis. Journal of Hydrology: Regional Studies. **13**, 1, **2017**.
27. DU W.Y., HE R.X., HE S.Y., SUN P.A., MO J.Y., QIN X.X., YU S. Variation of hydrochemical characteristics and the ion source in the upstream of Guijiang river: A case study in Guilin section. Carsologica Sinica. **36** (2), 207, **2017**.
28. YANG P.H., YUAN D.X., YUAN W.H., KUANG Y.L., JIA P., HE Q.F. Formations of groundwater hydrogeochemistry in a karst system during storm events as revealed by PCA. Chinese Science Bulletin. **55**, 1412, **2010**.